International Journal of Solids and Structures 000 (2015) 1–8

Contents lists available at ScienceDirect

International Journal of Solids and Structures

journal homepage: www.elsevier.com/locate/ijsolstr

Optimal structural arrangements of multilayer helical assemblies

Nikolaos Karathanasopoulos [a,*], Panagiotis Angelikopoulos [b]

[a] Institute for Mechanical Systems, ETH Zürich, Leonhardstrasse 21, CH-8092 Zürich, Switzerland
[b] Chair for Computational Science, ETH Zürich, Clausiusstrasse 33, CH-8092 Zürich, Switzerland

ARTICLE INFO

Article history:
Received 29 April 2015
Revised 6 August 2015
Available online xxx

Keywords:
Helical assembly
Optimal design
Numerical simulation
Axial strain

ABSTRACT

We report a quantitative framework to guide the braiding pattern design of multilayer helical assemblies. We optimize the structural pattern so as to maximize the construction's resistance to axial loads and concurrently minimize its torsional propensity. To that extent, we consider helical assemblies comprised of up to five layers, for which we identify favorable structural patterns, providing a database that covers most practical applications.

1. Introduction

Helical assemblies are load carrying structures with applications ranging from ropes and electricity power transfer cables to tissue engineering scaffolds (Papailiou 1997; Laurent et al., 2014). While a large number of studies has been devoted to the analysis of their mechanical properties, the selection of the structural arrangement itself has largely been disregarded, despite its rather detrimental impact on both the operational mechanical response and the structure's long term performance. Whereas an experimental retrieval of optimal structural patterns is infeasible, numerical simulations provide an ideal test-bed for this purpose.

A thorough description of the geometric properties of single, double and triple helical bodies has been provided by Lee (Lee, 1991), an analysis of primal use for the understanding of the structuring of helical assemblies. Helical assemblies are commonly encountered as substructures of larger constructions. Cable-bridge structures are characteristic examples of this kind, for which the cable tension level and placement controls the response of the overall construction (Janjic et al., 2003). Furthermore, helical assemblies are used in electric power transfer, with their design playing a crucial role in the minimization of power transfer losses (Sullivan, 1999). Their extensive use necessitated the characterization of their mechanical response, as the analytical and numerical modeling schemes bibliography indicates, primarily in the context of engineering cables.

Using analytical modeling, Lanteigne provided closed-formed solutions for the quantification of the mechanical response of helically armored cables upon axial, torsional and bending loads (Lanteigne, 1985). Accordingly, Raoof et al. developed simplified expressions for the stiffness coefficients of locked-coil strands (Raoof and Kraincanic, 1998), while Utting and Jones provided a large set of experimental data on single and three layer strands accompanied by closed-form stiffness expressions (Utting and Jones 1987a, 1987b). Furthermore, Costello conducted extensive experimental studies to characterize the mechanical response of wire ropes, complementing the experimental analysis with analytical, closed-form expressions for the structural response (Costello, 1990). Moreover, Sathikh et al. elaborated stiffness matrix coefficients for the axial and torsional strain response of helical bodies that hold symmetry considerations of the stiffness matrix (Sathikh et al., 1996), while Karathanasopoulos et al. extended the modeling approach to account for the effect of radial strain with contributions arising from the axial, torsional and bending helix cross section stiffness taken into account (Karathanasopoulos and Kress, 2015). Finally, the mechanical response of double-helix multi strand constructions to axial and torsional loads was analyzed, under the assumption that their constituents follow a fiber type response (Elata et al. 2004; Usabiaga and Pagalday 2008).

On the numerical modeling side, Jiang et al. estimated the structural properties of two layer strands using a reduced computational model that took advantage of the structural and loading symmetry (Jiang and Henshall 2000). Similarly, Stanova et al. worked on the axial stiffness properties of three layered strands (Stanova et al., 2011). A study on large spiral cables axial load-strain curves and failure loads was provided by Judge et al., the analysis based on three dimensional finite element modeling (Judge et al., 2012).

More recently, helical assembly applications that go beyond the context of engineering strands have come to the fore. In particular,

* Corresponding author. Tel.: +41 44 633 6331; fax: +41 44 632 1145.
E-mail addresses: nkaratha@ethz.ch, karathanasopoulosn@gmail.com (N. Karathanasopoulos), panagiotis.angelikopoulos@mavt.ethz.ch (P. Angelikopoulos).

http://dx.doi.org/10.1016/j.ijsolstr.2015.09.023
0020-7683/

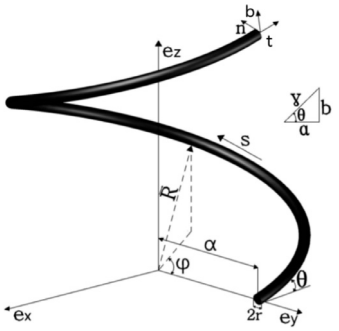

Fig. 1. Helical body geometry.

in the field of biomechanical engineering, helically braided scaffolds have been used for the restoration of tendon and ligament tissue (Laurent et al., 2014). Moreover, the development of artificial and biological material based applications such as nanotube helical ropes, has asked for a deeper understanding of their mechanical response, with bottom-up structural response models appearing in the literature (Zhao et al., 2014).

A significant number of studies have been devoted to assess the impact of loading bounds on the endurance and long-term functionality of helical assemblies. Argatov worked on the effect of inter-wire contact deformation of single layer rope strands making use of asymptotic modeling (Argatov, 2011). Alani et al. studied the correlation between the mean axial loading and the endurance limits of helical assemblies, to point out substantial variations associated with the helix angle selection of the individual layers (Alani and Raoof, 1997). Giglio et al. (Giglio and Manes, 2005) derived a linkage between the fatigue life and the stress state of ropes that are subject to axial and bending loads, suggesting that their bounds are directly related to fretting damage phenomena (Hobbs and Raoof, 1994). Finally, Chaplin performed a number of experimental studies that quantified the effect of different loading patterns on the life endurance of spiral ropes, illustrating the role of torsional loads as a failure mechanism (Chaplin, 2008).

The current work is structured as follows: We describe the engineering of a broad spectrum of helical assembly constructions comprised of up to five layers (Section 2). Amongst all possible structures, we identify torsionally counterbalanced arrangements of high axial stiffness for two, three, four and five layer constructions (Section 3, Appendix A). We comment on the retrieved optimal braiding patterns and conclude in Section 4.

2. Helical assembly modeling and optimization methodology

2.1. Helix geometry

The geometry of the helical assembly is characterized by the individual geometric properties of its constituents. A helix can be described through the following equation, formed with the use of the *Serret–Frenet* basis:

$$\mathbf{X}(x_n, x_b, s) = \begin{Bmatrix} X \\ Y \\ Z \end{Bmatrix} = \mathbf{R}(s) + x_n\mathbf{n} + x_b\mathbf{b}, \quad -r \le x_n, x_b \le r \tag{1}$$

where r denotes the radius of the helix cross section and $\mathbf{R}(s)$ the centerline position vector of the helical body defined as follows:

$$\mathbf{R}(s) = \begin{Bmatrix} \alpha\cos\varphi \\ \alpha\sin\varphi \\ b\varphi \end{Bmatrix}, \quad \varphi = \frac{s}{\gamma}, \quad \gamma = \sqrt{\alpha^2 + b^2},$$
$$b = \alpha\tan\theta, \quad h = 2\pi b \tag{2}$$

In Eq. 2, a stands for the helix centerline position and b for the rise along the central axis of the helix per unit angular evolution φ upon which the helix height h for a period evolution is computed. The *Serret–Frenet* local base vectors are defined as follows:

$$\mathbf{n} = \begin{bmatrix} -\cos\varphi \\ -\sin\varphi \\ 0 \end{bmatrix}, \quad \mathbf{b} = \frac{1}{\gamma}\begin{bmatrix} b\sin\varphi \\ -b\cos\varphi \\ \alpha \end{bmatrix}, \quad \mathbf{t} = \frac{1}{\gamma}\begin{bmatrix} -\alpha\sin\varphi \\ \alpha\cos\varphi \\ b \end{bmatrix} \tag{3}$$

Fig. 1 schematically depicts the introduced parametrization.

2.2. Multilayer helical assembly parameter search space

We subsequently define the parameter space of the helical assemblies. For each helical layer, the cross section radius of the individual helical bodies r_i is allowed to vary by a maximum of 50% with respect to the radius of the core of the structure r_c, thus $0.5 \le r_i/r_c \le 1.5$. The layer centerline position of each layer i, named as a_i is defined as a function of the radius of all helical bodies in the different layers j, $\{r_j\}_{j=1}^{i}$ and of the core radius r_c, as schematically illustrated in Fig. 2. The helix angle of each layer θ_i is accordingly considered to vary within $[70^\circ\ 85^\circ]$. The angle selection allows for the constituents of the assembly to be primarily subject to normal rather than shearing stresses, while it guaranties a high axial strength for the overall construction. Furthermore, we allow for different layer orientation

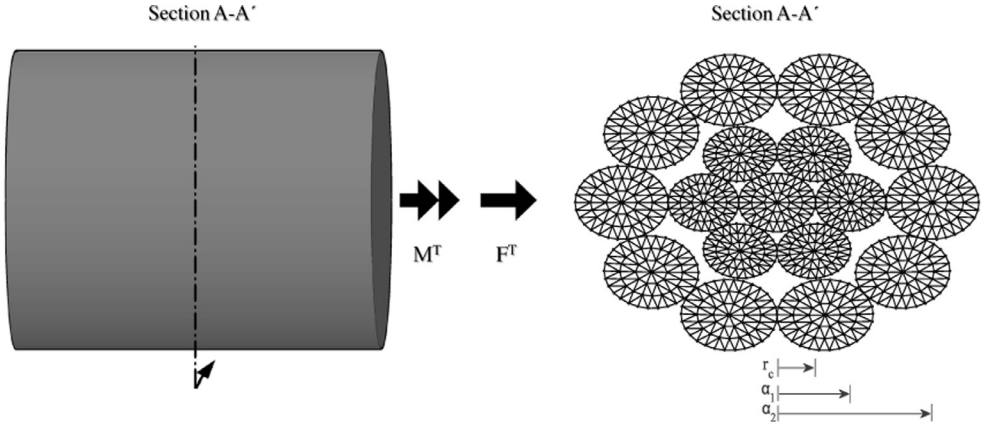

Fig. 2. Multilayer helical assembly geometry.

Please cite this article as: N. Karathanasopoulos, P. Angelikopoulos, Optimal structural arrangements of multilayer helical assemblies, International Journal of Solids and Structures (2015), http://dx.doi.org/10.1016/j.ijsolstr.2015.09.023

Table 1
Range of parameters considered for the different layers.

Layer i	θ_i (°)	α_i/r_c	N_i	Or_i
Core	90	/	1	/
1st	[70 85]	[1.5 2.5]	[5 9]	+/–
2nd	[70 85]	[2.5 5.5]	[8 28]	+/–
3rd	[70 85]	[3.5 8.5]	[10 45]	+/–
4th	[70 85]	[4.5 11]	[12 64]	+/–
5th	[70 85]	[5.5 14]	[14 80]	+/–

Table 2
Two, three and four layer assembly considered orientation combinations.

	Two layer	Three layer	Four layer
Orientation combinations	+ –	– + + + – + + + –	+ – + + + + – + + + + – – – + + + – – + + – + –

Table 3
Five layer assembly orientation combinations.

Orientation combinations	+ + – + + + + + – + + + + + – – – + + +	+ – – + + + + – – + + + + – – – + – + +	– + + – + – + + + – + – + – + + – + + – + + – + –

combinations Or_i. Each layer can follow either a right or a left handed directionality (+/−).

The left part of Fig. 2 depicts a two layer helical assembly with its internal structuring illustrated at the right hand side of the graph. The Section *A-A′* is a section normal to the axis *Z* along which the helical assembly develops:

The geometric search space bounds for each of the parameters are summarized in Table 1 for helical assemblies comprised of up to five layers. The limiting number of helical bodies N_i positioned at each layer can be readily retrieved upon trigonometric considerations elaborated in Section 2.3.

The orientation combinations studied for a two, three and four layer assembly are enlisted in Table 2.

Respectively, the orientation combinations for a five layer structure are summarized in Table 3.

It needs to be noted that equi-directional combinations have been excluded as no torsionally balanced constructions can arise. Furthermore, opposite polarity orientation combinations with respect to the enlisted ones have not been taken into account, since the minimization of the total arising moment is of sole interest.

2.3. Geometrically feasible constructions

We constrain the parameter space of the layered arrangements so as to allow only for compact constructions in their radial and circumferential braiding pattern. Since the retrieval of the feasible constructions is non-trivial, we provide a calculation scheme that obtains the geometric boundaries of the helical bodies.

The helix boundaries can be demarcated by the intersection of the *Cartesian* plane Z=0 with Eq. 1, which yields:

$$\begin{Bmatrix} X \\ Y \end{Bmatrix} = (\alpha - x_n)\begin{Bmatrix} \cos\varphi^* \\ \sin\varphi^* \end{Bmatrix} + x_b \frac{b}{\gamma}\begin{Bmatrix} \sin\varphi^* \\ -\cos\varphi^* \end{Bmatrix}, \quad \varphi^* = -\frac{\alpha}{b\gamma}x_b \tag{4}$$

The circumferential margin C' of the helix intersection with plane $Z = 0$ is subsequently calculated. To that extent, the local cross section coordinates (x_n, x_b) of the point C' are computed using the tangent point C of the circular helix cross section (Fig. 3 a), as follows:

$$\theta_{cp} = \arcsin\frac{r}{\alpha}, \quad \theta'_{cp} = 90^o - \theta_{cp}, \quad |x_n| = r\cos\theta'_{cp},$$
$$|x_b| = r\sin\theta'_{cp} \tag{5}$$

The bounds of each helical body are thereafter obtained through the central angular domain 2ψ (Fig. 3 b) formed by the margins of the above defined area (Eq. 4):

$$2\psi = 2\arctan\left(\frac{|Y_c|}{|X_c|}\right) \tag{6}$$

The central angular domain is subsequently used to determine the geometric parameter space combination $(\alpha_i/r_c, \theta_i, N_i)$ for which a complete layer is formed. More specifically, for a certain helix index value α_i/r_c, the values of θ_i are computed for which the division of a complete angle 2π with the central angular domain 2ψ yields integer values corresponding to the number of wires N_i for which a complete layer is formed. In Fig. 4 we illustrate the structuring of the feasible helical arrangements:

The analysis has been conducted with the following parameter discretizations. The helix angle θ° has been discretized with a step of 0.01° while the helix index α_i/r_c using a 0.001 step for the first innermost layer and a 0.01 step for all subsequent layers apart from the outermost, fifth layer, for which a 0.1 step has been used. In the resulting discrete feasible parameter space, the possible states are already in the order of tens of thousands for two layer constructions, following an exponential increase with each additional layer introduced. To retrieve the optimal constructions (Section 2.5), we exhaustively computed the structural response of all arising structures

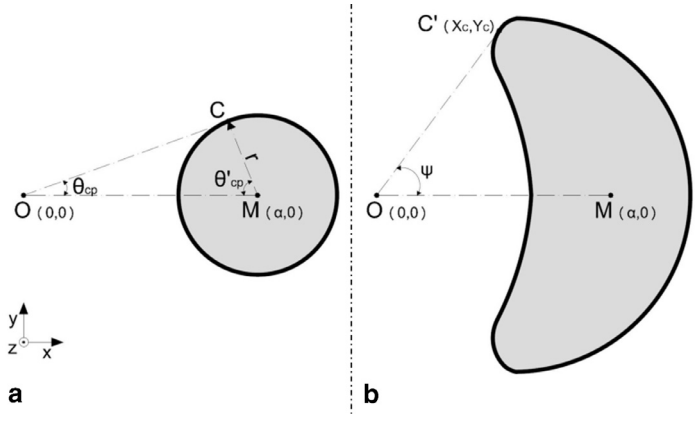

Fig. 3. Geometric bounds: (a) cross section, (b) helical body.

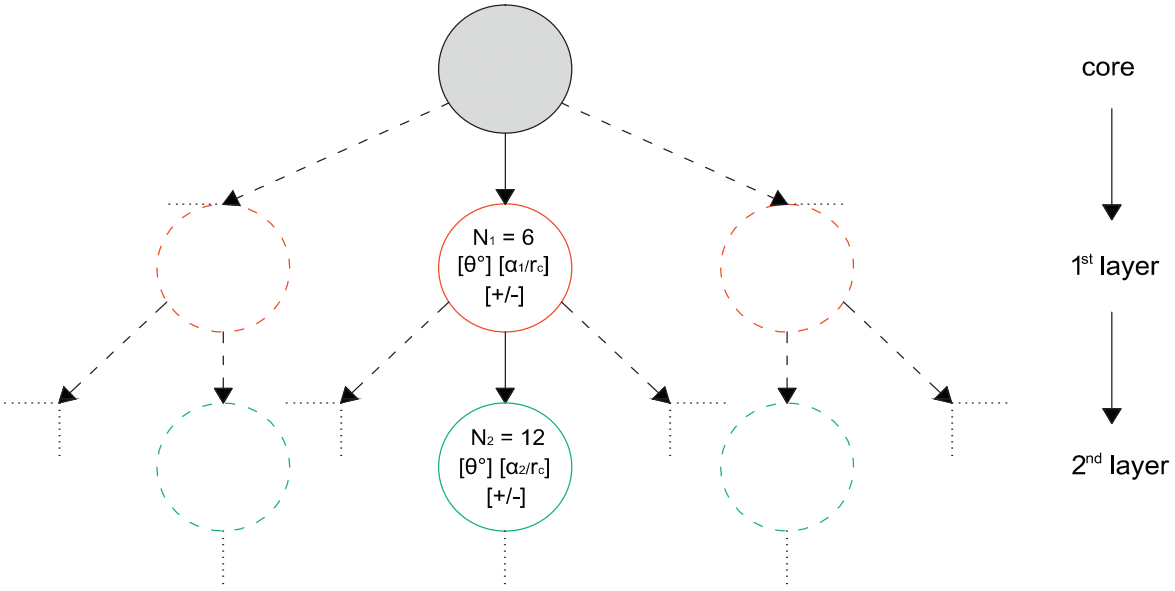

Fig. 4. Tree diagram representation of feasible construction paths.

(Section 2.4) in order to allow for a search of the entire parameter space (Brute force search). The approach readily allows us to perform a thorough statistical assessment of the favorable layer orientation combinations as elaborated in Section 3.1.

2.4. Helical assembly mechanical modeling

The different helical assembly structural arrangements have been parametrically constructed setting the core radius r_c to unity. The total axial force F^T and moment M^T developed along the central axis Z of the helical assembly (Fig. 2) is calculated superposing the contributions of the construction's constituents for each helical layer, as follows:

$$F^T = F_{core} + \sum_{i=1}^{k} N_i F_i^z, \quad M^T = \sum_{i=1}^{k} N_i M_i^z O r_i \tag{7}$$

where the contribution of the central core is given as $F_{core} = EA_c\epsilon_z = E\pi\epsilon_z$, E being the elastic material modulus and ϵ_z the axial strain applied, defined as $\epsilon_z = \delta h/h$. The axial force and moment contribution F_i^z and M_i^z of each helical constituent is computed with the use of analytical, closed-form expressions provided in (Karathanasopoulos and Kress, 2015). The corresponding expressions are provided for completeness below:

$$\begin{aligned} F_i^z &= \left(EA_i s^3 + \frac{EI_i}{\alpha_i^2} s^3 c^4 + \frac{GJ_i}{\alpha_i^2} s c^6\right)\epsilon_z \\ M_i^z &= \left(EA_i \alpha_i c s^2 - \frac{EI_i}{\alpha_i} s^2 c^3 (1+s^2) + \frac{GJ_i}{\alpha_i} s^4 c^3\right)\epsilon_z \end{aligned} \tag{8}$$

In Eq. 8, A_i, I_i and J_i stand for the geometric attributes of the cross section of a helical body positioned at layer i, namely for the helix cross sectional area, the second moment and the polar moment of inertia ($I_i = \pi r_i^4/4$, $J = 2I$). Moreover, c and s stand for the $\cos\theta_i$ and $\sin\theta_i$ respectively (θ_i being the helix angle of a wire positioned at layer i, Fig. 1), while α_i stands for the centerline position of the helix (Eq. 2).

For the computations, the linear elastic material modulus E appearing in Eq. 8 has been set to unity, while the *Poisson* ratio was set to $\nu = 0.3$ for the shear modulus G to be computed ($G = E/(2(1+\nu))$). The computations have been made for a linear strain $\epsilon_z = 0.01$. Finally, we note that Eq. 7 neglects any friction between the wires.

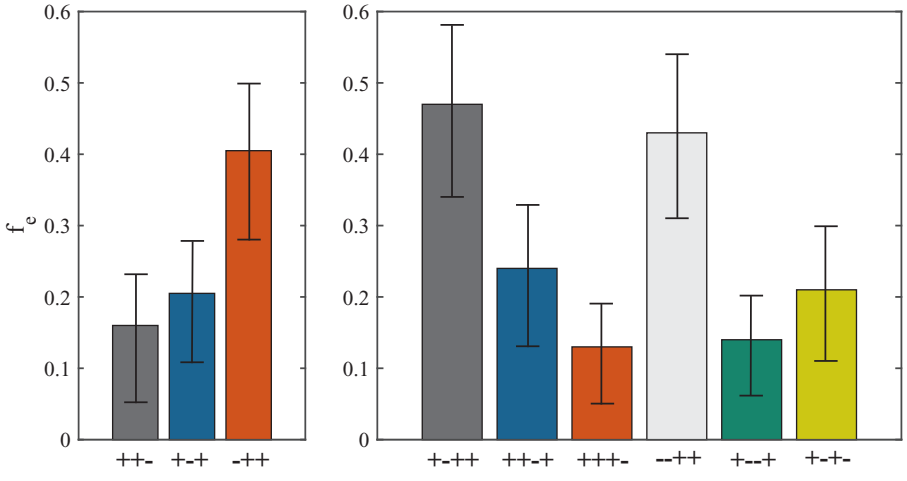

Fig. 5. Efficiency factor statistics for three (left) and four (right) layer constructions.

Please cite this article as: N. Karathanasopoulos, P. Angelikopoulos, Optimal structural arrangements of multilayer helical assemblies, International Journal of Solids and Structures (2015), http://dx.doi.org/10.1016/j.ijsolstr.2015.09.023

2.5. Helical assembly optimality criteria

The identification of favorable structural arrangements hinges upon the following structural objectives. We favor structures that

1. **Maximize** the axial stiffness $\kappa_A^h = \frac{F^T}{\epsilon_z}$, or respectively its normalized counterpart κ_A^{*h}, with the normalization carried out with respect to the stiffness of a rod of the same total cross sectional area and material (EA^R).
2. **Minimize** the resulting moment M^T, or respectively its normalized form $M^* = \frac{M^T}{M^T_{Max}}$, where M^T_{Max} is the maximum arising total moment within the considered structural arrangements, discretely for a two, three, four or five layer structure.

The above objectives (o) can be written as follows:

$$o = \begin{cases} \kappa_A^{*h} = \kappa_A^h / EA^R & (\uparrow) \\ M^* = M^T / M^T_{Max} & (\downarrow) \end{cases} \tag{9}$$

Assuming equal weights amongst the two structural objectives, we can combine them in the form of an *efficiency factor* f_e that is defined as the quotient of the normalized moment over the normalized axial stiffness of the structural arrangement:

$$f_e = \frac{M^*}{\kappa_A^{*h}} \quad (\downarrow) \tag{10}$$

The above factor allows for a classification of the different structural patterns, where favorable constructions are characterized by efficiency factors that approach zero. To avoid sub-optimal axial stiffness constructions, we bound the normalized axial stiffness to be above 0.85.

3. Optimal structural arrangement patterns

3.1. Favorable layer orientation combinations

In order to quantify the effect of the different layer orientation combinations, we present statistics on the respective efficiency factors f_e. Regarding two layer constructions, the efficiency factor mean value is $\bar{f}_e = 0.39$ with its inter-quantile range being $[f_{e|0.25}\ f_{e|0.75}] = [0.22\ 0.53]$. As regards three and four layer constructions, the mean efficiency factor values $\bar{f}_e$ and inter-quantile ranges are presented in Fig. 5.

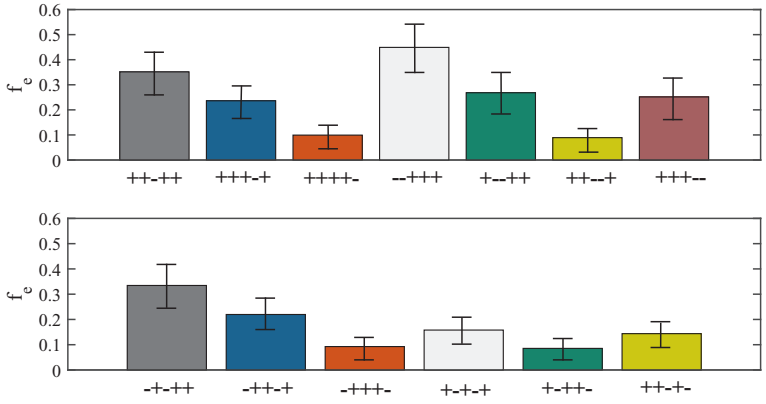

Fig. 6. Efficiency factor statistics for five layer constructions.

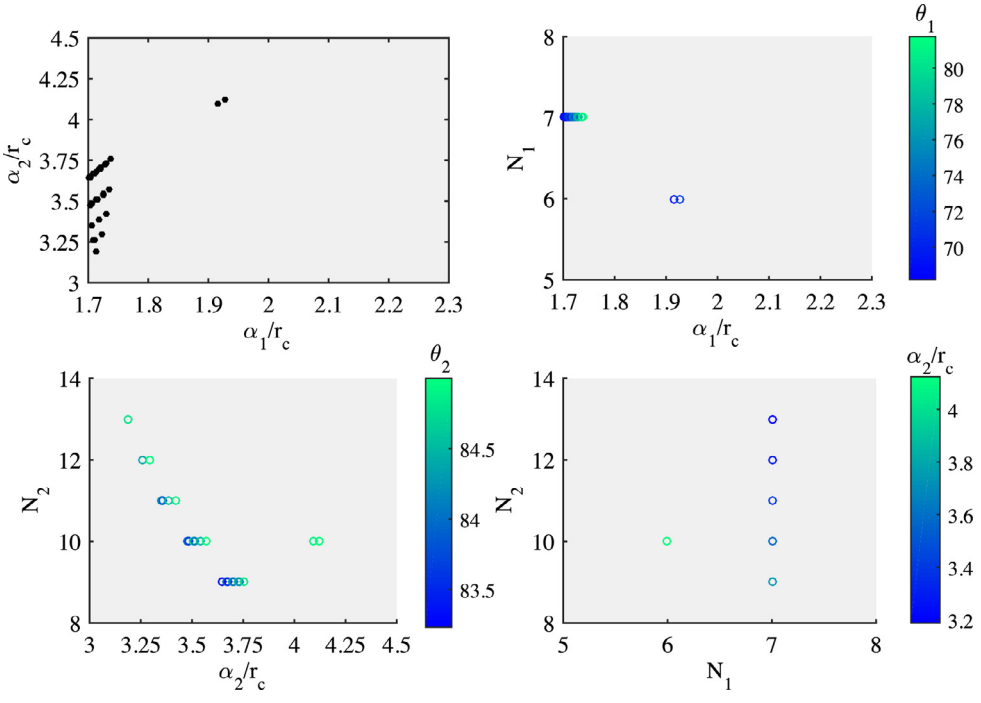

Fig. 7. Two layer assembly optimal structural patterns.

Please cite this article as: N. Karathanasopoulos, P. Angelikopoulos, Optimal structural arrangements of multilayer helical assemblies, International Journal of Solids and Structures (2015), http://dx.doi.org/10.1016/j.ijsolstr.2015.09.023

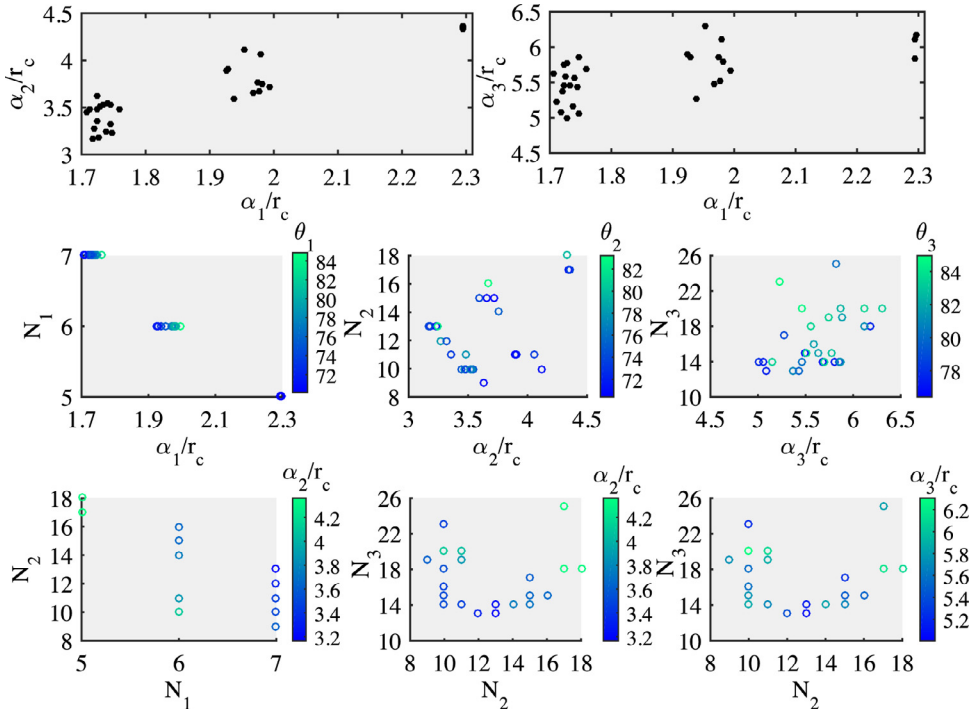

Fig. 8. Three layer assembly optimal structural patterns, orientation combination ++–.

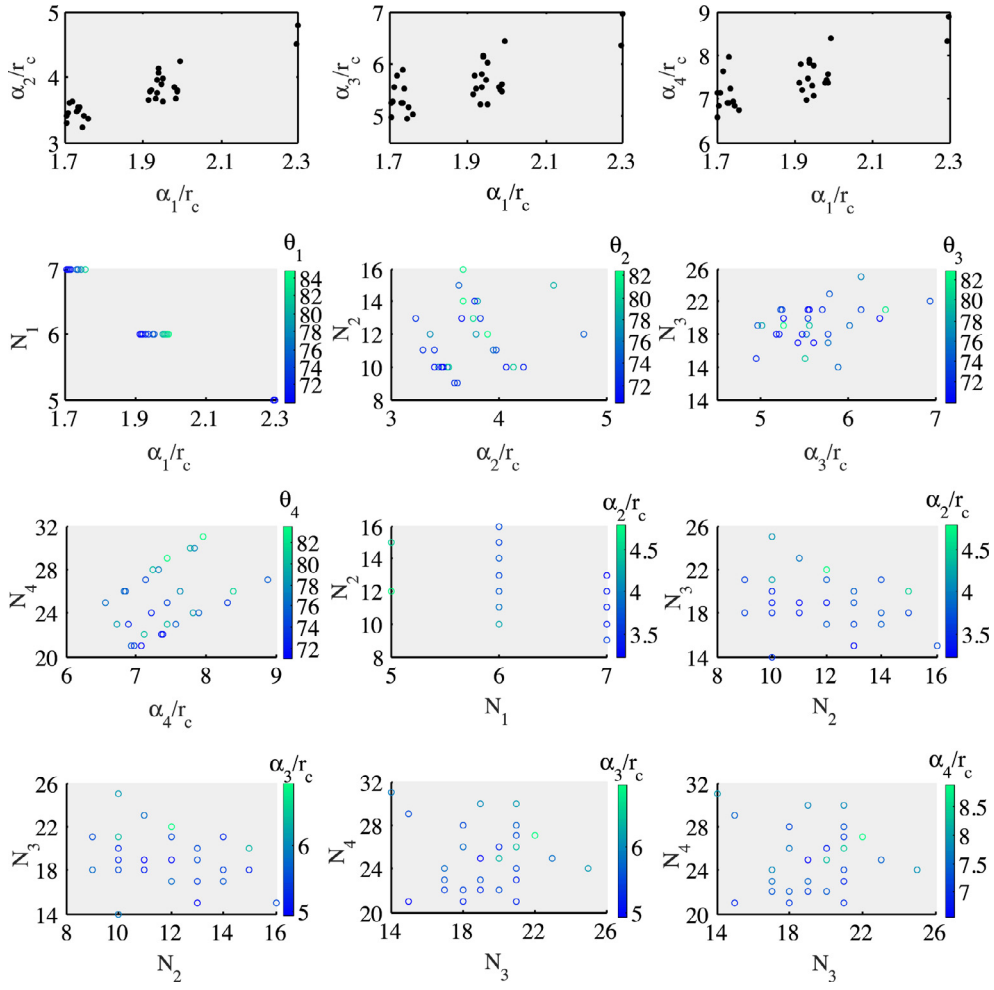

Fig. 9. Four layer assembly optimal structural patterns, orientation combination +++–.

Please cite this article as: N. Karathanasopoulos, P. Angelikopoulos, Optimal structural arrangements of multilayer helical assemblies, International Journal of Solids and Structures (2015), http://dx.doi.org/10.1016/j.ijsolstr.2015.09.023

The respective values for five layer assemblies are depicted in Fig. 6.

In Sections 3.2–3.4 as well as in the Appendix A, we provide a subset of optimal structural patterns. The full set of the identified favorable structural arrangements is provided as supplementary material.

3.2. Two layer construction

In Fig. 7 favorable two layer constructions with corresponding efficiency factor values f_e in the lowest 2% quantile are depicted.

3.3. Three layer construction

In Fig. 8 we present favorable three layer constructions with efficiency factor values f_e in the lower 0.5% quantile for two inner equi-directional layers followed by an outermost layer of opposite directionality:

3.4. Four layer construction

In Fig. 9 we portray favorable four layer constructions with efficiency factor values f_e in the lowest 0.01% quantile for the layer orientation combination of three inner equi-directional layers enclosed by an opposite directionality outermost layer.

3.5. On the optimality bounds of helical assemblies comprised of layers with helical bodies of quasi-equal cross section radius

In certain applications (e.g. engineering metallic strands (Stanova et al., 2011), quasi-equal cross section radius values (r_i) have been employed, up to a 2% difference with respect to the core radius. Tables 4 to 7 provide favorable structural arrangements for up to five layer helical assembly constructions in the above reduced parameter space:

It needs to be noted that even though the above structural patterns are the optimal constructions identified in the above constrained parameter space, their efficiency factor values are more than three orders of magnitude worse than the absolute optimal ones retrieved for the entire parametric space (Table 1).

Table 4
Two layer assembly.

List	a_1/r_c	$\theta_1(^\circ)$	N_1	a_2/r_c	$\theta_2(^\circ)$	N_2	Or
1	1.984	81.60	6	4.00	84.31	12	+ –

Table 5
Three layer assembly.

List	$a_{1\|2\|3}/r_c$	$\theta_{1\|2\|3}(^\circ)$	$N_{1\|2\|3}$	Or
1	1.983|3.96|5.96	81.34|74.72|77.38	6|12|18	+ + –

Table 6
Four layer assembly.

List	$a_{1\|2\|3\|4}/r_c$	$\theta_{1\|2\|3\|4}(^\circ)$	$N_{1\|2\|3\|4}$	Or
1	1.986|4.00|6.03|8.03	82.15|83.72|72.43|83.34	6|12|18|25	+ + – +
2	1.994|4.02|6.04|8.03	84.86|81.79|84.90|83.59	6|12|19|25	+ + + –

Table 7
Five layer assembly.

$a_{1\|2\|3\|4\|5}/r_c$	$\theta_{1\|2\|3\|4\|5}(^\circ)$	$N_{1\|2\|3\|4\|5}$	Or
1.991|4.01|6.01|7.98|9.98	83.71|82.5|78.5|73.6|73.3	6|12|19|24|30	+ + + + –
1.991|4.00|6.00|7.98|9.98	83.71|79.6|82.7|73.6|82.0	6|12|19|24|31	+ – + – +

4. Discussion and conclusions

An efficiency quantification of the different layer orientation combinations has been provided in Figs. 5 and 6, designating the structurally favorable weaving patterns. The figures suggest that structuring the helical assembly upon layers of alternating directionality does not yield on average the most favorable constructions, as the torsional moment counterbalancing is non linearly dependent on the associated geometric parameters.

Furthermore, Figs. 7–9 illustrate that constructions made up of layers of quasi-equal helix cross sections do not yield efficiency factors in the same order of magnitude as the optimal retrieved ones. In other words, extending the design parameter space constitutes a necessity for optimal helical constructions to be retrieved, while resorting to constructions comprised of four or five layers not only broadens the available optimal design constructions but allows for the engineering of constructions of considerably low efficiency factors.

It should be noted that even though the current study provides a complete enumeration of favorable structural arrangements of up to 5 helical layers, covering most practical applications, extension to structures of a higher layering is also feasible. However, the feasible parameter space increases exponentially with each additional layer, making a brute force calculation of optimal patterns computationally intractable. One would then have to use dynamic optimization techniques to explore the hybrid discrete-continuum parameter search space such as reinforcement learning (Gosavi, 2009), extensions which are outside the scope of the current work .

In the current analysis we employed equal weights amongst axial loading efficiency and torsional counter balancing, as dictaded by the definition of the efficiency factor. However, an introduction of weights amongst the two objectives is possible so as to tailor accordingly the selection of the optimal structural pattern.

The selection of the structural pattern constitutes a primal design step with a considerable impact on the functionality and endurance of the helical assembly. An optimal structural pattern yields a lower internal loading that allows for the minimization of related fatigue and wear phenomena. Such a design leads to the improvement of the mechanical performance and the prolongation of the structure's life expectancy, attributes strongly related to cost effective structural solutions.

To conclude, we presented a scheme for the quantification and selection of favorable structural patterns. Helical assembly constructions of up to five layers were parsed for the favorable parameter space to be identified, furnishing an extended database of optimal structural arrangements that covers a wide range of practical applications. We anticipate the current work to function not only as a reference but also as a general working framework in the optimization of helical assembly constructions.

Acknowledgments

NK acknowledges support by the Swiss National Science Foundation under project no. 200021-137544-1. PA acknowledges support from the European Research Council (Advanced Investigator Award No. 341117- PI Petros Koumoutsakos). We would also like to thank Dr. M. F. Vassiliou for fruitful discussions.

Appendix A. Optimal structural arrangements

The most favorable structural arrangements retrieved upon the hereby considered parametric space for a three layer helical assembly are provided in Table A.8.

Accordingly, a list of the most favorable structural arrangements retrieved upon the hereby considered parametric space for a four layer helical assembly is provided in Table A.9

Table A.8
Three layer assembly optimal structural arrangements.

List	$a_{1\|2\|3}/r_c$	$\theta_{1\|2\|3}(^\circ)$	$N_{1\|2\|3}$	Or
1	1.517|2.80|4.50	84.85|76.56|83.13	9|11|15	+ + –
2	2.372|4.62|6.93	77.40|77.05|82.54	5|16|15	+ – +

Table A.9
Four layer assembly optimal structural arrangements.

List	$a_{1\|2\|3\|4}/r_c$	$\theta_{1\|2\|3\|4}(^\circ)$	$N_{1\|2\|3\|4}$	Or
1	1.966|4.23|6.14|7.75	77.72|83.43|78.96|81.15	6|10|31|24	+ + – +
2	1.730|3.31|4.81|6.36	75.12|82.58|71.54|71.51	7|12|22|21	+ + + –
3	2.393|4.76|6.74|9.05	80.18|78.55|73.23|74.46	5|15|20|21	+ – – +
4	1.580|3.06|4.49|6.42	72.32|71.28|78.23|78.23	8|10|26|14	+ – + –

Table A.10
Five layer assembly optimal structural arrangements.

$a_{1\|2\|3\|4\|5}/r_c$	$\theta_{1\|2\|3\|4\|5}(^\circ)$	$N_{1\|2\|3\|4\|5}$	Or
1.721|3.94|6.94|9.14|11.04	73.35|83.4|75.8|72.0|76.0	7|8|14|39|28	+ + + – +
1.517|2.78|4.72|6.81|8.41	84.85|72.3|76.3|75.8|78.8	9|11|12|23|37	+ + + + –
1.708|3.09|4.32|5.78|7.48	71.06|77.0|83.7|71.0|81.7	7|14|24|19|29	+ + – – +
2.321|4.37|6.15|8.40|10.30	72.32|73.8|79.2|73.2|84.7	5|18|18|21|46	+ – + – +
1.916|3.78|5.64|7.45|9.45	71.53|75.6|78.3|74.4|74.8	6|12|19|25|26	+ – + + –

Finally, favorable structural patterns for a five layer construction are provided in Table A.10.

Supplementary material

Supplementary material associated with this article can be found, in the online version, at 10.1016/j.ijsolstr.2015.09.023

References

Alani, M., Raoof, M., 1997. Effect of mean axial load on axial fatigue life of spiral strands. Int. J. Fatigue 19 (1), 1–11.
Argatov, I., 2011. Response of a wire rope strand to axial and torsional loads: asymptotic modeling of the effect of interwire contact deformations. Int. J. Solids Struct. 48 (10), 1413–1423.
Chaplin, C.R., 2008. Interactive fatigue in wire rope applications, keynote lecture. In: Proceedings of Symposium on mechanics of slender structures (MoSS 2008). Baltimore, USA, pp. 1–12.
Costello, G., 1990. Theory of wire rope. Springer.
Elata, D., Eshkenazy, R., Weiss, M., 2004. The mechanical behavior of a wire rope with an independent wire rope core. Int. J. Solids Struct. 41 (5-6), 1157–1172.
Giglio, M., Manes, a., 2005. Life prediction of a wire rope subjected to axial and bending loads. Eng. Fail. Anal. 12 (4), 549–568.
Gosavi, A., 2009. Reinforcement learning: a tutorial survey and recent advances. Inf. J. Comput. 21 (2), 178–192.
Hobbs, R., Raoof, M., 1994. Mechanism of fretting fatigue in steel cables. Int. J. Fatigue 16 (4), 273–280.
Janjic, D., Pircher, M., Pircher, H., 2003. Optimization of cable tensioning in cable-stayed bridges. J. Bridge Eng. 8 (3), 131–137.
Judge, R., Yang, Z., Jones, S., Beattie, G., 2012. Full 3D finite element modelling of spiral strand cables. Const. Building Mater. 35, 452–459.
Karathanasopoulos, N., Kress, G., 2015. Mechanical response of a helical body to axial, torsional and radial strain. Int. J. Mech. Sci. 94â??95, 260–265.
Lanteigne, J., 1985. Theoretical estimation of the response of helically armored cables to tension, torsion, and bending. J. Appl. Mech. 52 (2), 423–432.
Laurent, C.P., Latil, P., Durville, D., Rahouadj, R., Geindreau, C., Orgéas, L., Ganghoffer, J.-F., 2014. Mechanical behaviour of a fibrous scaffold for ligament tissue engineering: finite elements analysis vs. *X*-ray tomography imaging. J. Mech. Behav. Biomed. Mater. 40, 222–233.
Lee, W., 1991. An insight into wire rope geometry. Int. J. Solids Struct. 28 (4), 471–490.
Papailiou, K., 1997. On the bending stiffness of transmission line conductors. IEEE Transactions on Power Delivery, 12 (4), 1576–1588.
Raoof, M., Kraincanic, I., 1998. Prediction of coupled axial/torsional stiffness coefficients of locked-coil ropes. Comput. struct. 69 (1), 305–319.
Sathikh, S., Moorthy, M.B.K., Krishnan, M., 1996. A symmetric linear elastic model for helical wire strands under axisymmetric loads. J. Strain Anal. Eng. Des. 31 (5), 389–399.
Stanova, E., Fedorko, G., Fabian, M., Kmet, S., 2011. Computer modelling of wire strands and ropes part II: finite element-based applications. Adv. Eng. Softw. 42 (6), 322–331.
Sullivan, C.R., 1999. Optimal choice for number of strands in a litz-wire transformer winding. IEEE Transactions on Power Electronics 14 (2), 283–291.
Usabiaga, H., Pagalday, J., 2008. Analytical procedure for modelling recursively and wire by wire stranded ropes subjected to traction and torsion loads. Int. J. Solids Struct. 45 (21), 5503–5520.
Utting, W., Jones, N., 1987a. The response of wire rope strands to axial tensile loads—Part I. Experimental results and theoretical predictions. Int. J. Mech. Sci. 29 (9), 605–619.
Utting, W., Jones, N., 1987b. The response of wire rope strands to axial tensile loads-part II: comparison of experimental results and theoretical predictions. Int. J. Mech. Sci. 29 (9), 621–636.
W.G. Jiang and J.L. Henshall, 2000. A novel finite element model for helical springs. Finite Elem. Anal. Des. 35, 363–377.
Zhao, Z.L., Zhao, H.P., Wang, J.S., Zhang, Z., Feng, X.Q., 2014. Mechanical properties of carbon nanotube ropes with hierarchical helical structures. J. Mech. Phys. Solids 71 (1), 64–83.

Please cite this article as: N. Karathanasopoulos, P. Angelikopoulos, Optimal structural arrangements of multilayer helical assemblies, International Journal of Solids and Structures (2015), http://dx.doi.org/10.1016/j.ijsolstr.2015.09.023